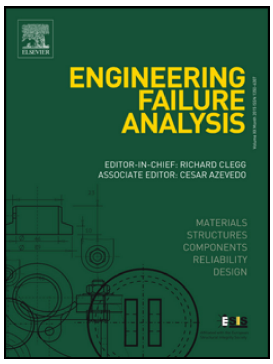

Seismic behavior of 1960's RC buildings exposed to marine environment

David Bru, Antonio González, F. Javier Baeza, Salvador Ivorra

PII: S1350-6307(18)30065-7
DOI: doi:10.1016/j.engfailanal.2018.02.011
Reference: EFA 3377

To appear in: *Engineering Failure Analysis*

Received date: 13 January 2018
Revised date: 7 February 2018
Accepted date: 19 February 2018

Please cite this article as: David Bru, Antonio González, F. Javier Baeza, Salvador Ivorra , Seismic behavior of 1960's RC buildings exposed to marine environment. The address for the corresponding author was captured as affiliation for all authors. Please check if appropriate. Efa(2017), doi:10.1016/j.engfailanal.2018.02.011

Seismic behavior of 1960's RC buildings exposed to marine environment.

David Bru[1], Antonio González[1], F. Javier Baeza[1], and Salvador Ivorra [1]*

[1] *Department of Civil Engineering, University of Alicante. San Vicente Del Raspeig, Apartado 99, 03080, Spain*

** Corresponding author. Tel.: +34 965903707; Fax: +34 96 590 3678. E-mail: sivorra@ua.es*

ABSTRACT

Steel rebars corrosion is one of the most important problems of reinforced concrete (RC) structures. The mechanical performance loss of RC elements because of steel corrosion can be aggravated under horizontal loads (e.g. wind pressure or seismic actions). This paper presents a methodology for the study of the seismic behavior of a residential typology of the Mediterranean coast, which was widely spread during the 1960's. These RC frame structures are usually 10 to 15 stories high, located very close to the coast and are exempt buildings, which made them specially exposed to chloride corrosion. Besides, there are some design conditions that should be taken into account: (i) these structures were designed only under gravity loads, especially seismic actions were not considered. (ii) The raw materials had lower quality than those considered in current design codes, e.g. structural concrete strength was around 15 MPa, and made with natural beach sand as fine aggregates (hence including chlorides into the concrete mass). Therefore, two important aspects converge in these buildings, fifty years of marine exposure (i.e. degradation by corrosion) and the omission of the seismic loads in the original design, making them especially vulnerable to earthquakes (in an area with a moderate-high seismicity). Hence, a methodology for the seismic analysis of the corroded structure is proposed, in order to determine the structural safety factor of this type of structures, and evaluate the effectiveness of a retrofitting if necessary.

Keywords: Seismic loads; plastic hinge; vulnerability; RC building corrosion; marine environment

1. Introduction.

The great explosion of tourism in the Valencian coast at the end of the 1950's, caused the urbanization of a great area of the littoral. This urban development prioritized the views and proximity to the sea. Therefore, the architectural design tried to optimize the orientation and views limiting the closed areas, hence large perimeter cantilevered balconies were a basic feature as solariums. The rationalist architect Juan Guardiola-Gaya was one of the main protagonists of this architecture in the early 1960's. He is responsible for the current architectural image of the Costa Blanca from Alicante to Benidorm. Fig. 1 includes some examples of this building typology, like the development of Albufereta Beach or the Vistamar tower (inspired by the Pirelli Tower in Milan by Pier Luigi Nervi). All these buildings have a common set of characteristics: compact and regular plans, façades facing the sea with large balconies supported by cantilever beams, reinforced concrete (RC) frame structures with flat beams, and direct marine spray exposure. Besides, this area of Spain presents a medium to high seismic activity according to current design codes [1]. The recent earthquake that heavily affected the city of Lorca in 2011 is an example, in which peak ground accelerations up to 0.36 g were recorded [2]. As a summary, these constructions present some common aspects that highly increase their seismic vulnerability: (i) All buildings are inhabited and the economic value of these apartments is higher than other neighborhoods. (ii) The original structure was made in poor quality RC (characteristic compressive strength f_{ck} lower than 17.5 MPa), and without any prescription regarding durability. (iii) Their structural capacity has been degraded after several years of marine spray exposure. (iv) During their design horizontal seismic loads were not considered. Therefore, in this

seismic area there is a large building stock, apartment blocks more than 10 stories high, which present some pathologies (cracks and spalling due to steel corrosion of RC elements) after 50 years of marine exposure, and have been designed without any seismic code considerations.

Figure 1. Mediterranean Spanish Coast, landscape of Albufera area (Alicante).

The current Spanish seismic design code [1], classifies the area of the South and East of the Iberian Peninsula as a medium to high grade level seismic zone. Therefore, specific seismic design of structures is mandatory. However, these criteria have only been applied in the last two decades. Before that, buildings were designed only under vertical loads and horizontal wind forces. In fact, the first Spanish standard that considered seismic actions was not published until 1962 [3], and only affected buildings in areas with at least level VII on the Mercalli scale, which were only a couple southern areas, Figure 2. Nonetheless, the area of study remained outside and was considered a non-seismic area. Hence, the presented aspects motivate a specific analysis of the seismic effects on the 1960's coastal buildings in this area.

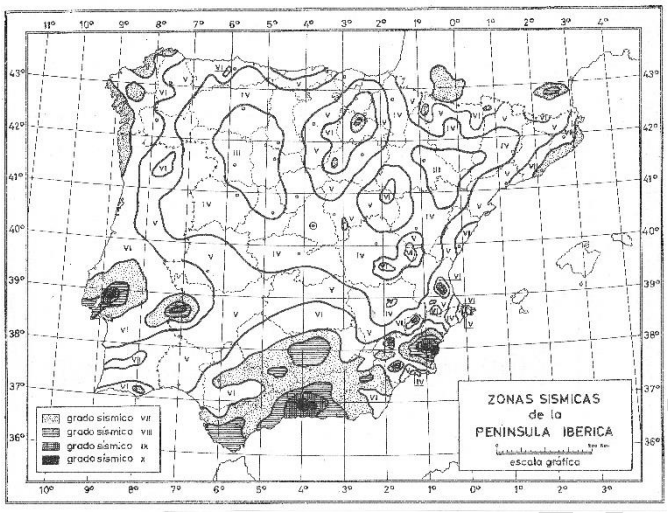

Figure 2. Seismic hazard map of 1962 Spanish standard.

The problematic related to structural degradation, because of corrosion, in constructions located in seismic prone areas is currently being studied [4], and usually requires from complex models. The effect of steel corrosion in RC structural elements is one of the fundamental durability problems in concrete constructions, and has been widely studied [5]. The damage magnitude depends on the material's properties and design conditions, i.e. rebar's coating, and environmental exposure conditions. In the particular case of coast nearby constructions, the two main corrosion types are carbonation and chloride induced corrosion (caused by marine environment). In this sense, Tuuti [6], proposed a model for the service life of RC structures, which comprised two different stages. The first one, or initiation phase, lasts until the aggressive substances (carbon dioxide or chloride ions) get to the steel surface at a concentration higher enough to depassivate it, and hence corrosion begins. Afterwards, the second stage, or propagation phase, considers the time during steel is actually damaged, with the corresponding mechanical properties loss, and lasts until the end of the structural service life.

The effect of steel corrosion on the mechanical properties of RC structures has been widely studied. Several researchers report the residual properties of corroded rebars [7,8], the induced concrete cover cracking [9] or the rebar-concrete bonding after

corrosion [10,11]. Also the influence of corrosion on structural elements subject to cyclic loading has been experimentally assessed [12,13], even for the seismic evaluation of structures [14]. Finally there are complex numerical approaches to model the corrosion of steel rebars in concrete and the cover cracking or spalling.

Therefore, the main objective of this paper is aimed at a simplified methodology for the seismic analysis of RC buildings exposed to marine environment corrosion. In addition, the proposed method was applied to residential buildings (taller than 8 floors) built in 1960's in the East coast of Spain, which after more than 50 years show signs of steel corrosion that could affect their seismic performance (especially considering that they were designed without any specific seismic analysis, and the poor quality materials were used). This analysis considers the non-linear behavior of RC under seismic loads, and the level of structural degradation due to chloride exposure over five decades. Non-linear pushover analysis [15] will be addressed according to different Standards [16], [17], [18], in which structural degradation is simulated by modified non-linear characteristics of materials (as a function of the exposure time to marine environment).

2. Methodology.

The aim of this paper is to evaluate the seismic behavior of a specific structural typology, widely spread in the East coast of Spain in the 1960's, directly exposed to marine environment, and located in a seismic-prone area. First, a brief description of the structural characteristics considered in this work has been included. After the procedure used to evaluate the corrosion of RC elements is described. Finally, the numerical method to perform the seismic analyses is presented.

2.1. Description of the general RC Building model of 1960's.

Figure 3 includes different examples of the typical 1960-70's buildings in the East coast of Spain. In general, they can be classified in two different types, depending on the

existence or not of concrete walls on the staircases and elevator shafts. Nonetheless, they weren't supposed to increase the seismic safety factor, the stiffness increase was only to control the maximum horizontal displacements due to wind actions.

Figure 3. Typical apartment buildings in Alicante. (a) Adoc Tower 10, (b) Adoc Tower 7 and (c) Vistamar tower,

A real building of fifteen floors (Figure 3b) has been selected as an example of these constructions, and has been used to illustrate the proposed methodology. The general structural scheme of *Adoc Tower 7* is presented in Figure 4. The plan presents structural symmetry with seven parallel frames with spans between 3.30 and 4.30 m. The total frame length is 3.65 m and the height of columns is 2.60 m. Table 1 summarizes the main characteristics of the cross sections of beams (BS), columns (CS) and walls (WS). Mechanical characteristics of each section have been calculated assuming 15 MPa concrete and plain steel bars with 400 MPa yielding stress. Main frames are composed by 50x20 cm² flat beams, connected by 15x20 cm² perimeter beams, and unidirectional slabs (with secondary beams each 80 cm). In order to account for the effect of the concrete slabs in the global structural model, the recommendations of Calavera [19] and Darwell & Allen [20] have been considered. Thus, an equivalent virtual 30x20 cm² secondary beam was defined directly connecting columns on consecutive frames. Columns have a constant 30x40 cm² cross section up to the eighth floor (23.4 m) and progressively decreases upwards until 25x25 cm² at the top floor (41.6 m). The only

exception are the columns aligned with the concrete walls, which maintain a constant 30x40 cm² section for all stories. There are three concrete walls, one 30x210 cm² on the elevator shafts (WS-1), and two 25x100 cm² on the staircases (WS-2).

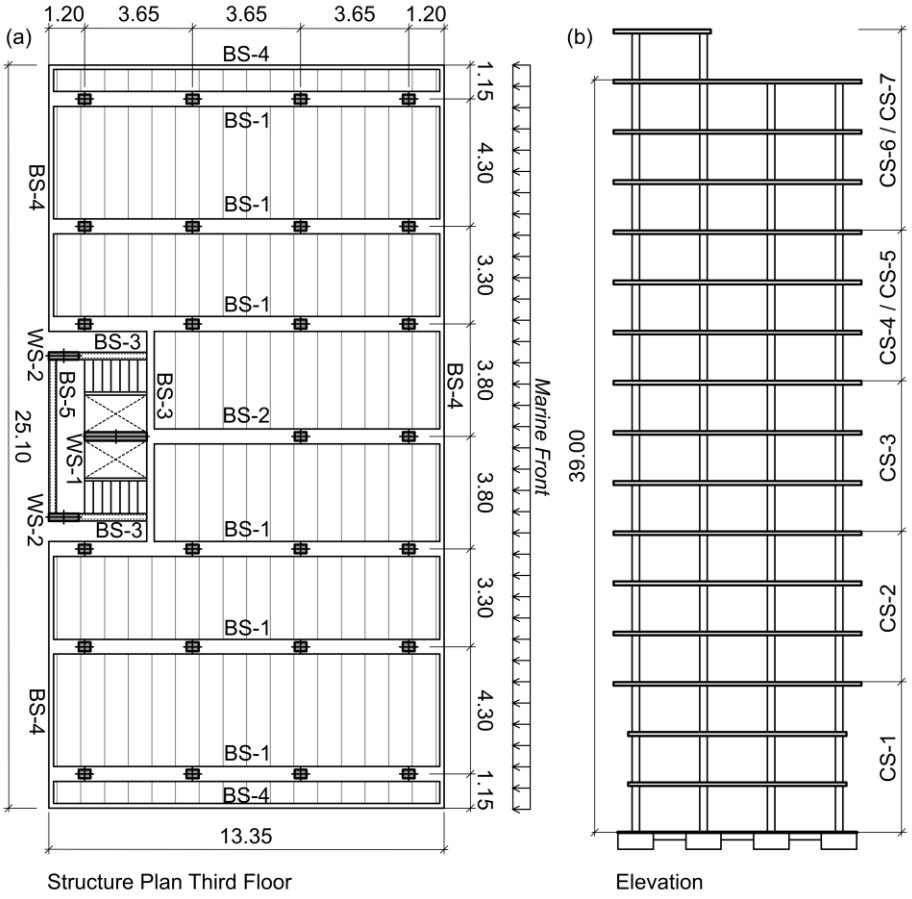

Figure 4. General structural scheme (a) XY view, (b) YZ elevation view.

Table 1. Main geometric and mechanical characteristics of all RC structural sections.

Type	Geom.	Top	Bott.	Stirrups	Yield. Mom.	Plastic Mom.	Ult. Shear Force	Idealized Yield curvature	Plastic curvature	Plastic rotation capacity
-	cm	mm	mm	mm	kN·m	kN·m	kN	rad/m	rad/m	rad
CS-1	30x40	4∅25	4∅25	∅8/200	307.0	321.8	152.0	0.0136	0.0057[c]	0.0012
CS-2	30x40	4∅20	4∅20	∅8/200	243.8	247.9	143.9	0.0142	0.0098[c]	0.0020
CS-3	30x40	3∅16	3∅16	∅6/150	150.6	155.9	109.3	0.0122	0.0195 [c]	0.0039
CS-4	30x30	3∅16	3∅16	∅6/150	127.1	133.9	109.3	0.0108	0.0266[s]	0.0053
CS-5	30x30	3∅16	3∅16	∅6/150	89.1	93.1	88.9	0.0167	0.0350[c]	0.0052
CS-6	30x40	2∅14	2∅14	∅6/120	58.8	60.9	110.5	0.0084	0.0246[s]	0.0049
CS-7	30x30	2∅14	2∅14	∅6/120	32.7	33.9	86.9	0.0170	0.0461[s]	0.0069
BS-1	50x20	8∅16	6∅16	∅6/200	68.9 -89.4	70.1 -91.1	84.4	0.0208 0.0240	0.0589[s] 0.0380[c]	0.0059 0.0038
BS-2	50x20	9∅20	5∅20	∅6/200	87.0	88.1	97.2	0.0212	0.0576[c]	0.0058

					-147.3	-148.6		0.0309	0.0082[c]	0.0008
BS-3	25x20	2∅14	2∅14	∅6/200	18.4	18.9	37.0	0.0188	0.0566[s]	0.0057
BS-4	15x20	2∅10	2∅10	∅6/200	19.02	18.9	21.0	0.0203	0.0570[s]	0.0057
BS-5	30x20	6∅12	6∅12	∅6/200	39.5	40.3	52.3	0.0208	0.0576[c]	0.0058
WS-1 *	30x210	5∅16	5∅16	∅6/150+28∅6 ***	2870.2	3525.7	459.1	0.0021	0.0050[s]	0.0052
WS-2 **	25x100	4∅12	4∅12	∅6/150+12∅6 ***	551.4	648.6	223.2	0.0045	0.0101[c]	0.0051

* Lateral reinforcement equal to 12 ϕ16 in both sides.
** Lateral reinforcement equal to 12 ϕ16 in both sides.
*** Interior reinforced rebars parallel to 30cm side.
Note: The medium axial load for gravity loads was selected for the evaluation of the plastic behavior.
[c] maximum curvature limited by concrete crushing.
[s] maximum curvature limited by steel strain.

2.2. Corrosion analysis of RC elements exposed to marine environment.

The time analysis of RC corrosion requires a two stage process, initiation and propagation phases according to the aforementioned model proposed by Tuuti [6]. For the first one, many Standards have different models for the ingress of aggressive agents through the concrete pore network, in order to estimate the time necessary to initiate corrosion. In this work, the Spanish concrete design code has been adopted, which is based on the second Fick's law, Eq. (1), in which for a time of exposure *t* in years, the depth of penetration of the aggressive agent *d*, is function of the coefficient of diffusion *K*.

$$d = K \cdot \sqrt{t} \tag{1}$$

The diffusion coefficient depends on the type of agent (CO_2 or Cl^-), and the respective coefficients K_C and K_{Cl} can be assessed with Eq. (2), or Eq. (3), for carbonation or chloride ions ingress.

$$K_c = c_{env} \cdot c_{air} \cdot a \cdot f_{cm}^{b} \tag{2}$$

$$K_{Cl} = 56157 \cdot \sqrt{12 \cdot D(t)} \cdot \left[1 - \sqrt{\frac{C_{th} - C_b}{C_s - C_b}}\right] \tag{3}$$

$$D(t) = D(t_0).\left(\frac{t_0}{t}\right)^{0.5} \tag{4}$$

For carbonation, Eq. (2), c_{env} depends on the ambient conditions (wet or dry); c_{air} is an air entrainment coefficient; a and b are parameters depending on the type of cement; and f_{cm} is the average compressive strength of the concrete. In the chloride ingress, Eq. (3), C_{th} is the chloride threshold (i.e. critical Cl^- dosage by cement mass); C_b is the chloride amount included in the batch, which depends on the raw materials (aggregates, cement, water, admixtures and additions); and C_s is the Cl^- concentration on the concrete surface. Finally, to account for the time evolution of chloride diffusion, Eq. (4), $D(t)$ is the effective diffusion coefficient of Cl^- for a t age, and is expressed as a function of the diffusion coefficient obtained for a t_0 age, $D(t_0)$. The specific values of each parameter adopted in the present research are summarized in Table 2.

Table 2. Parameters for the assessment of diffusion coefficients in 2nd Fick's Law.

Carbonation						Chloride				
C_{anv}		C_{air}	a	b	f_{cm}	$D(t_0)$	n	C_{th}	C_s	C_b
Wet	Dry	-	-	-	MPa	cm^2/s	-	Cement mass %		
0.5	1	0.7	1800	-1.7	23	$1.77 \cdot 10^{-7}$	0.5	0.6	0.805	0.2-0.3-0.4

The propagation time t_p, which starts once aggressive agents have arrived to the steel rebars, is directly related to the corrosion level, which is affected by several factors [21], [22], [23]. There are different evaluation methods based on experimental, numerical or analytical models [24], [25], [26]. However, the Spanish standard EHE 08 [27] proposes a simplified expression, Eq. (5), in which the propagation time depends only on the coating thickness $d\,(mm)$, the rebar diameter $\emptyset\,(mm)$, and the corrosion velocity $V_{corr}\,(\mu m/year)$. Table 3 includes the results obtained applying this equation to different commercial diameters, depending on the type of exposure environment. Such values of generalized corrosion velocity are higher than the usual values, between 1 and

10 μm/year [28], considered for the study of corrosion, hence presenting a conservative situation. The values included in the Spanish code [27] establish a uniform damage accumulation along the steel rebars, generating a crack size increment, and the detachment of the concrete cover. However, due to the localized nature of chloride corrosion, the fissure opening would be lower [9]. Rodriguez et. al [29] propose different values of the local penetration factor, α, with the aim to evaluate the concrete crack process formation due to chloride attack [30]. In this case, the section loss caused by generalized carbonation induced corrosion will be characterized by α=2, while chloride corrosion will present α values between 4 and 8.

$$t_p = \frac{80}{\emptyset} \cdot \frac{d}{V_{corr}} \tag{5}$$

Table 3. Propagation time for maximum corrosion of steel rebars with 25mm cover in different ambient conditions.

Diameter	Propagation time (year)	
mm	IIIa $V_{corr} = 20\ \mu m/year$	IIa $V_{corr} = 3\ \mu m/year$
6	16.7	111.1
8	12.5	83.3
10	10.0	66.7
12	8.3	55.6
14	7.1	47.6
16	6.3	41.7
20	5.0	33.3
25	4.0	26.7

In order to quantify the mechanical performance loss of steel rebars during the propagation phase, four different variables were determined: (i) reduction of the cross section, (ii) variation of the yield strain, (iii) ultimate tensile load variation, and (iv) ductility loss. First, the steel thickness affected by corrosion P_x can be assessed using

Eq. (6) [28], as a function of the corrosion potential V_{corr} or intensity I_{corr}, and the time of exposure t_p. Then, the effect of the type of corrosion is considered to estimate the diameter loss, Eq. (7) [29], in which, ϕ and ϕ_0 are the final and initial rebar diameter, and α varies between 2 and 8, for homogeneous or pitting (chloride) corrosions. Afterwards, the level of corrosion Q_{corr}, Eq. (8), depends only on the diameter ratio of the corroded and original rebar. Finally, the variation of strength and strain can be obtained using Eq. (9) [7] and Eq. (10) [31], where F_u, F_{u0}, and ε_u, ε_{u0}, the values associated to the rebar mechanical capacity and ultimate strain, after and before corrosion. In addition, ε_u should be always higher than the effective yielding strain ε_y^* (obtained considering F_u and the reduced section because of corrosion).

$$P_x(mm) = 0.0116.\, I_{corr}.\, t_p = V_{corr}.\, t_p \tag{6}$$

$$\phi = \phi_0 - \alpha \cdot P_x \tag{7}$$

$$Q_{corr} = \left(1 - \left(\frac{\phi}{\phi_0}\right)^2\right) \cdot 100 \tag{8}$$

$$F_u = (1 - 0.014 \cdot Q_{corr}) \cdot F_{uo} \tag{9}$$

$$\varepsilon_u = (-0.269 \cdot \ln Q_{corr} - 0.21) \cdot \varepsilon_{u0} \geq \varepsilon_y^* \tag{10}$$

2.3. Nonlinear seismic analysis.

A 3D numerical model was made using the commercial software SAP2000 [32] to carry out non-linear static analyses to evaluate the seismic performance of the building and the effect of different levels of corrosion.

2.3.1. Seismic demand.

The seismic hazard has been determined according to the Spanish standard NCSE-02 [1]. The ground acceleration corresponding to the city of Alicante is 0.14 g (for a return period of 500 years). The actual location can be assumed as a soft subsoil condition (subsoil type III), according to geological and geotechnical available data [33], thus the

soil amplification factor (C) due to the site effect is equal to 1.6. Finally, a 5% damping ratio was assumed for concrete frame structures. Therefore, the response spectrum shows the maximum peak acceleration (0.435 g) for periods between 0.16 s and 0.435 s. Initially, a ductility level of 1 was considered, i.e. the seismic demand wasn't reduced due to ductility of RC sections.

2.3.2. Numerical analyses.

Pushover analyses were made to evaluate the nonlinear behavior of the building [34], [35]. In this method, the behavior of the building is assessed by means of capacity curves, which represent the relationship between the base shear force and the roof displacement for a lateral load distribution. Four load cases have been considered, accounting for the gravity loads and representative lateral load patterns, and two different corrosion-damaged scenarios were studied, for a total eight different analyses. According to EC-8 [16], ATC-40 [17] and FEMA 356 [18], the first load case is proportional only to the mass, therefore a uniform load distribution is applied (U). The second one considers lateral forces proportional to the product of mass and the first modal shape's amplitude at each story (M1). In an analogous way, the third and the fourth load patterns are proportional to the second (M2) and third (M3) modal shapes. In order to obtain the maximum modal roof displacement, the SRSS rule has been used to combine each modal response. These results are presented in the paper as Modal Pushover Analysis, MPA [36]. Second order effects were taken into account in all evaluated cases.

2.3.3. Nonlinear properties

The FE model was comprised by frame elements, and nonlinear behavior was considered due to large deformation effects and deterioration of concrete (compression cracking). Reinforced concrete material was defined by tension-compression curves

according to its confinement level. Figure 5 includes different stress-strain curves for unconfined (UC) and confined sections (C), as defined in Table 1, all values have been normalized with respect to the characteristic strength and strain values of UC concrete. UC sections assumed a parabolic curve according to EC-2 [37] indications, in which the compressive strength f_{ck} was equal to 15 MPa for a compressive strain $\varepsilon_{ck} = 2‰$. The elastic modulus considered in the first phase was 16.18 GPa, and the ultimate strain was 3.5‰ (i.e. a normalized 1.75 strain) for a compressive strength of 13 MPa. Tensile strength was 2.39 MPa with an ultimate tensile strain equal to 1.6‰. On the other hand, confined concrete (C), was evaluated according to the formulation proposed by Mander [38]. Figure 5 includes two different confined sections, CS-1 and WS-1 (Table 1), both of which showed improvements of compressive strength and ultimate strain. For example WS-1 section presented $1.2f_{ck}$ and $\varepsilon_{cu} = 2.25\varepsilon_{ck}$, because of the effect of the transverse rebars (parallel to the 30 cm side) that prevent the buckling of the longitudinal compressed rebars. Finally, all steel rebars were modelled as an elastoplastic material with 200 GPa elastic modulus, 411 MPa yielding stress, and 10‰ ultimate strain.

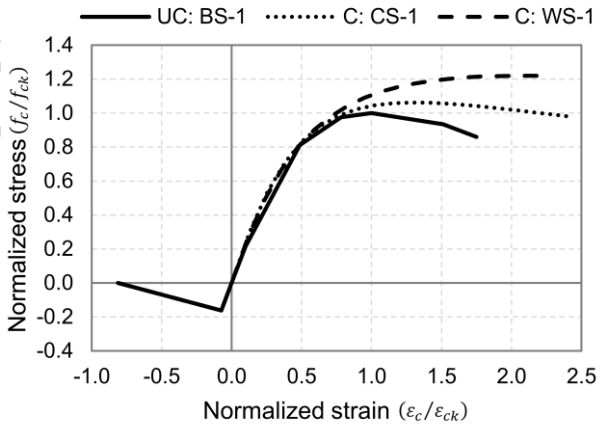

Figure 5. Examples of normalized confined (C) and unconfined (UC) stress-strain curves for different cross sections as defined in Table 1. Both magnitudes are divided by characteristic values of unconfined concrete.

The nonlinear behavior of RC sections was included by means of lumped plasticity on hinge elements at both ends of beams and columns. The characterization of these hinges

was made according to Inel and Ozmel [39], in which the mechanical behavior is defined by moment-rotation relationship. For this reason, the most critical parameters to fix are the moment-curvature relationship of each section, and the length of the hinge. Afterwards, the rotation can be calculated as the product of the section's curvature and the length of the hinge. In this research, the value of the hinge's length L_p was calculated as a function of section's depth H, $L_p = 0.5H$, according to Park & Pauly [40] and FEMA 356 [18]. This equation is simpler but gives more conservative values than others, e.g. $L_p = 0.08L + 0.022f_y\phi \geq 0.044f_y\phi$ [41] that considers the distance L as the critical distance from the critical section of the plastic hinge to the point of contraflexure. Figure 6 includes a diagram with the plastic hinge location following the seismic design recommendations of the California Department of Transportation (Caltrans) [42]. Additional shear hinges were located $L_p/2$ apart from their bending counterparts, according to concrete design code EHE-08 [27].

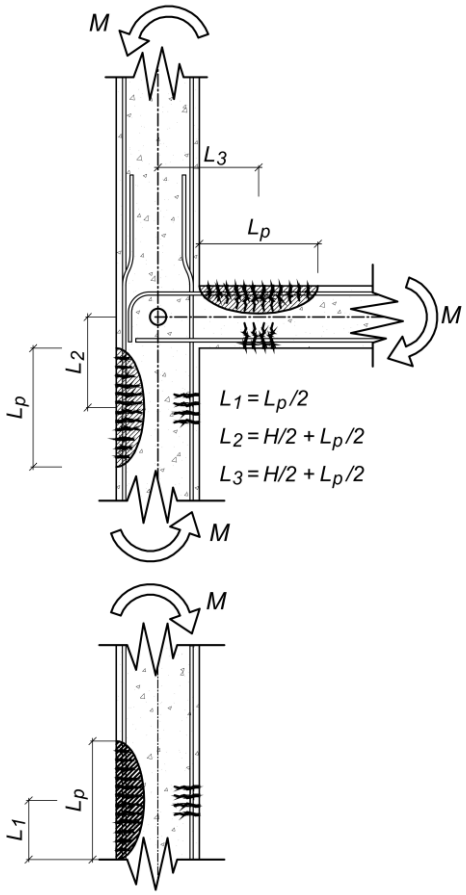

Figure 6. Geometrical position for plastic hinges.

Different moment-curvature diagrams were defined to consider axial-bending hinges in columns, and only bending hinges in beams. For this reason, the interaction diagram (axial-bending) and the moment-curvature diagram of each cross section was calculated for different axial loads, based on force equilibrium (axial and bending forces). Figure 7 includes an example of the monotonic backbone curve used in this research, in which φ_y and φ_{up} are the elastic and ultimate plastic curvatures respectively. Also, a simplified bilinear function, according to Caltrans standard [42], is included, where φ_{ip} is the equivalent plastic curvature. In particular, the $M-\varphi$ behavior has been modelled as the bilinear function in Figure 7, in which a final negative slope step (30% of elastic stiffness) was used to improve the convergence of the numerical models after $M_p-\varphi_{up}$ [43]. However, to control the global behavior of the plastic hinge in case of brittle

behavior, and in order to avoid the unreal behavior of the plastic hinge rotation, the maximum reduction of the bending moment was fixed at $0.2M_p$.

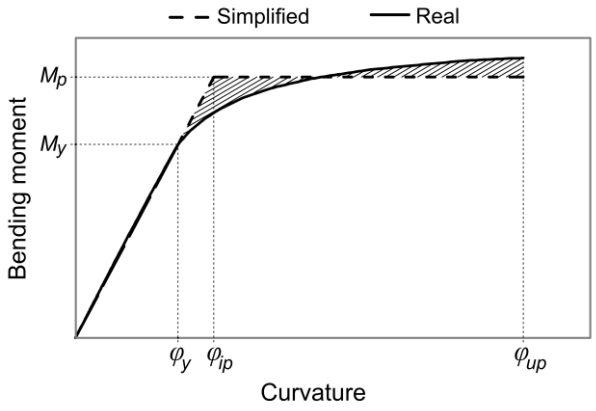

Figure 7. Moment curvature curve for RC sections.

These type of structures presented low concrete strength and an insufficient amount of transverse steel (as shown in Table 1), therefore the shear strength of RC sections should be considered. Hence, additional shear hinges were introduced in beams and columns to account for the loss strength and stiffness in the global behavior of the structure due to the shear collapse. Shear hinge properties were defined like linear springs with elastic properties until collapse. After this point, the member fails immediately, but to avoid several convergence problems in the numerical model, a 10% negative slope was defined. Shear strength was evaluated according to Spanish Concrete design code [27].

3. Results and discussion.

The methodology and analysis of results, is divided in the following steps: first, the corrosion damage was evaluated, and all structural elements were grouped into three corrosion level areas. Afterwards, the loss of mechanical properties was determined, and the numerical model updated. A modal analysis of the structure was performed together with a modal pushover to assess the global stability. Finally, local analyses of each

section was made to ensure that the ductility capacity of all hinges remained according to the model assumptions.

3.1 Corrosion.

First, the effect of corrosion on the mechanical properties loss of RC sections was evaluated. Figure 8 includes the time evolution of aggressive agents' penetration in concrete cover for different exposure conditions, according to EHE-08 [27]. Two different CO_2 scenarios (exposure condition type IIa) and three chloride initial contents C_b (exposure condition type IIIa) have been modeled. Also a 25 mm concrete cover has been represented, as the usual value for these coastal buildings in 1960's [44], [45]. The worst-case scenarios for each corrosion type were dry CO_2 and a 0.4% Cl^- content, which presented initiation times of 17 (CO_2) and 15 (Cl^-) years. If chloride concentrations were lower, this time interval would be increased up to 41 years or more.

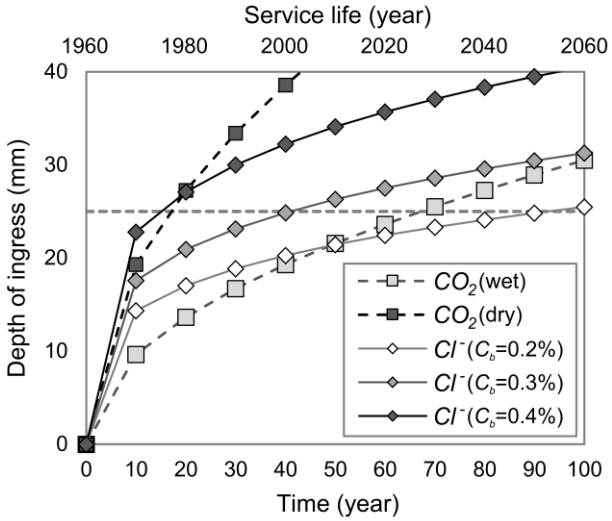

Figure 8. Time of penetration for initial corrosion phase

Once the propagation phase has begun, the diameter loss can be assessed applying the expressions in Eq. (6) to (10), included in section 2. Figure 9 summarizes the corrosion evolution in different conditions, i.e. carbonation ($V_{corr} = 3\ \mu m/year,\ I_{corr} = 0.258\ \mu A/cm^2$), and chloride corrosion ($V_{corr} = 20\ \mu m/year, I_{corr} = 1.724\ \mu A/cm^2$). Besides different penetration factors were assumed, e.g. α=2 for carbonation attacks,

α=4 for medium exposure chloride attacks (partially protected elements), and α=8 for structural elements highly exposed to marine environment (columns and beams in open balconies). The loss of diameter in carbonation-damaged rebars would be negligible considering the time intervals in this research. On the other hand, the structural elements exposed to medium or high Cl^- contents ($C_b = 0.3$ or $C_b = 0.4$) would have suffered 15 years (1a in Figure 9) or 40 years of corrosion, according to the results presented in Figure 8. Therefore, an effective diameter loss of 6.4 mm and 2.4 mm, (1c) in Figure 9, would have been produced respectively.

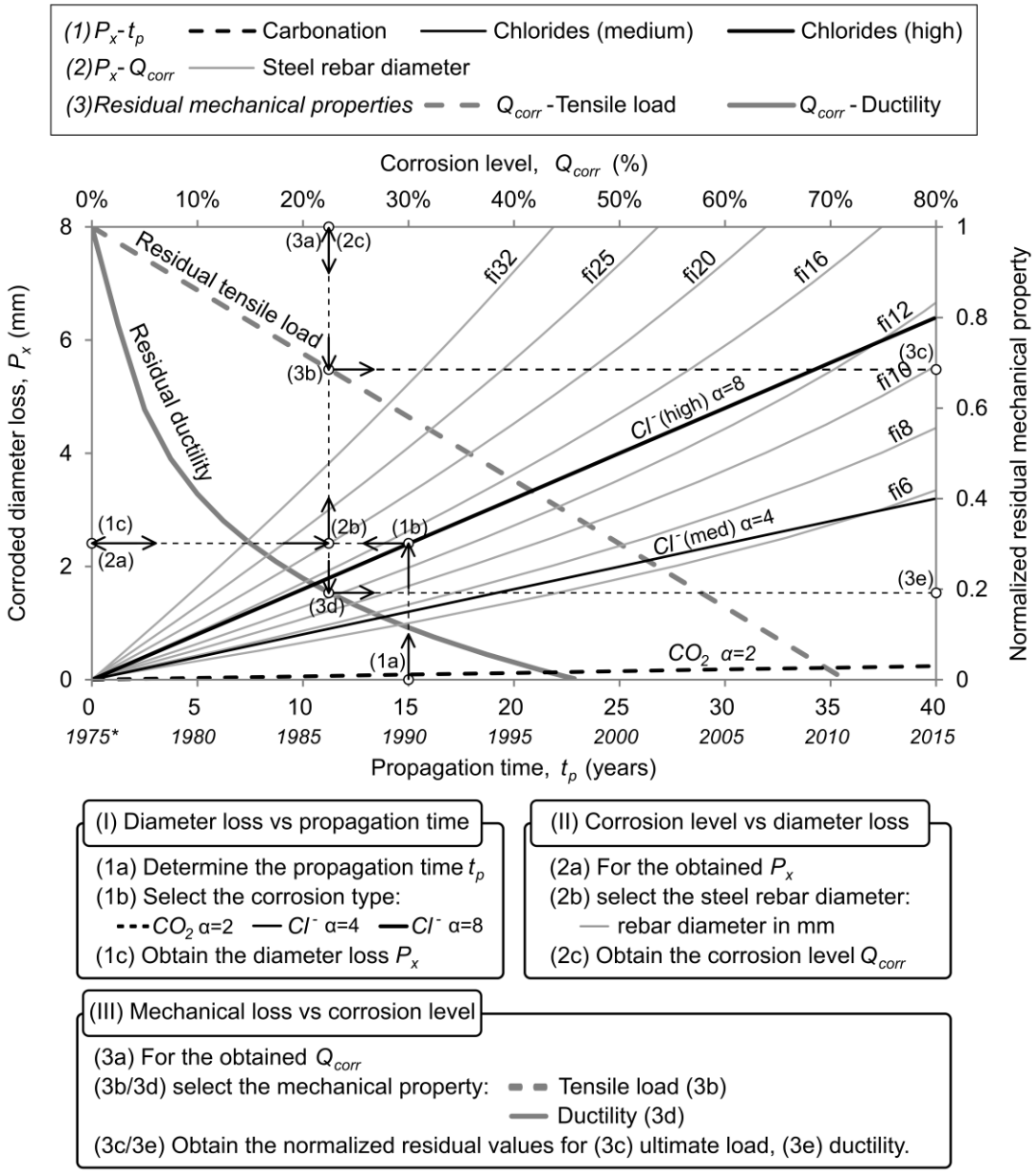

Figure 9. Evolution of the mechanical properties of reinforced steel rebars with the level of corrosion (* propagation time for the analyzed building, considering a 15-year initiation time since construction in 1960).

After, the section loss can be related to the corrosion level Q_{corr} depending on the actual steel diameter. As an example, point 2a in Figure 9 represents a 2.4 mm loss, which in a 20 mm rebar (2b), will correspond to a 23% Q_{corr} (2c). Finally, the normalized residual strength and ductility are presented versus the corresponding corrosion level. Once the corroded section has been determined, Eq. (6) in section 3.1, the level of corrosion Q_{corr} (3a) can be related to the ultimate tensile load F_u (3b) and strain ε_u (3d) of the corroded section according to Eq. (9) [7] and Eq. (10) [31], respectively. Both expressions only depend on the corrosion level Q_{corr} and the undamaged values F_{u0} and ε_{u0}. Hence, the 6.4 and 2.4 mm diameter loss obtained above would correspond to corrosion levels of 54 and 23%, whose corroded mechanical parameters would be $F_{u,Q=54\%} = 0.25\, F_{u0}, \varepsilon_{u,Q=54\%} = 0.0\, \varepsilon_{u0} \geq \varepsilon_y^*$ (hence there wasn't any plastic strain, and brittle failure would occur for effective yield strain ε_y^*) and $F_{u,Q=23\%} = 0.69\, F_{u0}, \varepsilon_{u,Q=23\%} = 0.19\, \varepsilon_{u0}$ (3c and 3e in Figure 9). These damaged mechanical properties, because of corrosion, can be observed in Figure 9 as a decrease in the mechanical capacity of rebars, and especially in the ductility of steel, as shown in [8]. The decrease of ε_u is important in seismic areas, in which the steel plastic deformation is limited to 10‰ to guarantee the design code conditions for ductile behavior of concrete sections. Therefore, the ductility reduction will be especially critical for a 33% level of corrosion, as the loss of global ductility would be 91.7%.

All structural elements were classified into three different areas of exposure for the seismic analyses, considering the aforementioned constructive characteristics of the studied buildings, whose mechanical properties were modified based on the curves included in Figure 9. This marine exposure distribution of the structural elements is represented in Figure 10, in which outer elements were considered in IIIa conditions

(zone 1 with α=8, and zone 3 with α=4), while inner elements were assumed as IIa ambient (α=2). Table 4 summarizes the mechanical properties reduction (as the ratio with respect the original value in Table 1) for each section affected by corrosion. These values were used in the seismic evaluation of the presented structural typology (residential tall buildings of 1960's), whose mechanical properties have been decreased by corrosion since 1975, and its seismic structural capacity could have been compromised.

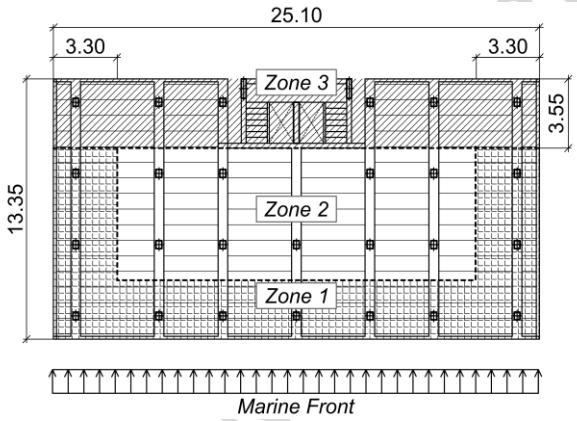

Figure 10. Areas of exposure considered for the structural analysis depending on the corrosion level.

Table 4. Representative relative modeling parameters for hinges under different corrosion levels since 1975.

	Zone I				Zone III			
Section	M_y/M_{y0}	M_p^*/M_{p0}	V/V_0	θ_p/θ_{T0}	M_y/M_{y0}	$M_p\ /M_{p0}$	V/V_0	θ_p/θ_{T0}
CS-1	0.449	0.428	0.671	0.304	0.748	0.736	0.671	0.910
CS-2	0.392	0.385	0.626	0.191	0.739	0.727	0.626	0.922
CS-3	0.379	0.366	0.687	0.076	0.739	0.735	0.687	0.693
CS-4	0.411	0.390	0.687	0.090	0.701	0.705	0.687	0.790
CS-5	0.346	0.331	0.688	0.068	0.701	0.701	0.688	0.676
CS-6	0.446	0.431	0.667	0.033	0.612	0.608	0.667	0.411
CS-7	0.493	0.475	0.687	0.026	0.625	0.621	0.687	0.412
BS-1	0.113 -0.115	0.112 -0.112	1	0.060 0.082	0.518 -0.523	0.524 -0.528	1.000	0.730 0.982
BS-2	0.264 -0.273	0.260 -0.271	1	0.120 0.293	0.611 -0.617	0.616 -0.626	1.000	0.990 1.476
WS-1*	-	-	-	-	0.737	0.703	0.592	0.767
WS-2**	-	-	-	-	0.701	0.596	0.664	0.182

Note: The medium axial load for gravity loads was selected for the evaluation of the plastic behavior.

[c], maximum curvature limited by concrete crushing.

[s], maximum curvature limited by steel strain.

* when the plastic bending moment in the corrosion model was 0, the elastic bending moment M_y was used.

3.2 Seismic load and dynamic properties.

Figure 11 includes four response spectra corresponding to different coastal cities (assuming identical geotechnical conditions), in which the aforementioned structural typology was widely used in the 1960's. Moreover, the periods corresponding to the main bending modes, either in x and y directions, are represented in Figure 11. Table 5 summarizes the results of the modal analysis, i.e. the calculated elastic fundamental periods, and the elastic demands for the RC frame model. According to different standards [18], [17], [16], and due to the regular modal behavior in both directions, only the direction of the principal frames has been used in this research, corresponding to the modes included in Figure 12. The modal analysis considered only the elastic properties of the structural model, therefore there wasn't any difference between the undamaged and corroded structures. Hence, it is worth noting that the corrosion effect only affects the nonlinear behavior of the structure.

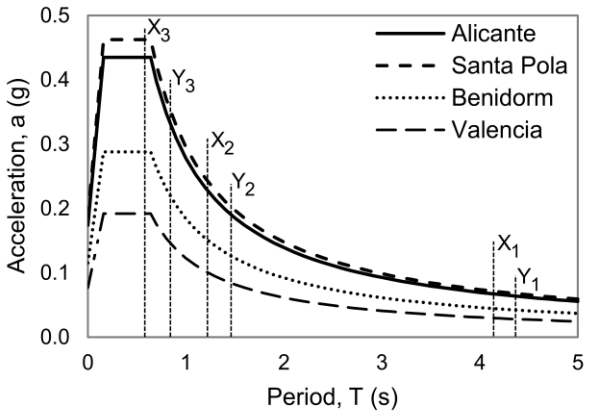

Figure 11. Elastic response spectrum for touristic urban areas in Spanish Mediterranean Coast, according to Spanish Seismic Code NCSE-02 [1].

Table 5. Modal properties and linear dynamic results according to NCSE 02 [1] for seismic actions in Alicante.

Mode	Period T	Mass ratio Ω	Modal participation factor, Γ	V_d^*	D^*	δ_0	Direction
	s	%	1/m	%	%	cm	x-y
Y_1	4.36	80.5	52.1	4.83	0.77	2.54	y

Y_2	1.46	9.60	18.0	1.83	0.26	2.89	y
Y_3	0.84	3.35	10.6	1.11	0.15	3.28	y
X_1	4.14	74.20	50.1	4.98	0.73	2.51	x
X_2	1.22	12.01	20.2	2.74	0.21	2.63	x
X_3	0.58	5.07	13.1	2.20	0.09	2.54	x

V_d^*, normalized lineal modal base shear response (i.e. base shear / total weight of the building).
D^*, normalized maximum modal roof displacement (i.e. modal roof displacement demand/total height).
$\delta_{0,}$ modal roof displacement for modal shape.

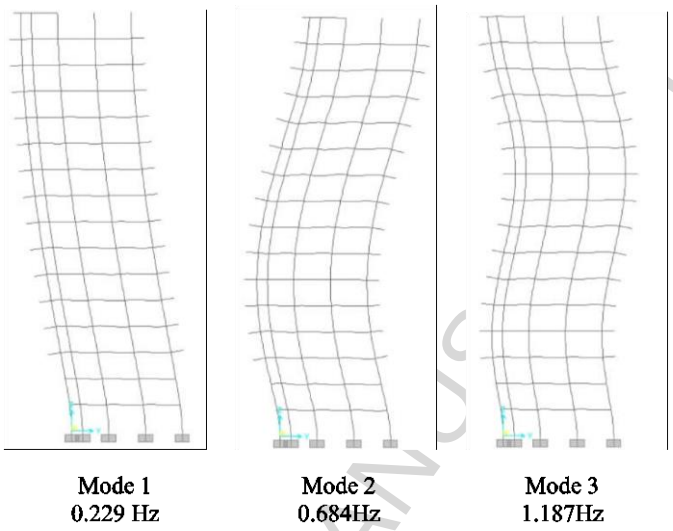

Figure 12. Modal shapes and frequencies for the first three modes in Y direction.

The real active mass during the seismic action was determined using the old Spanish standard MV-101, whose materials were similar to those used during the construction of the building, and the mass coefficients were selected according to the current design code NCSE-02. In particular, the selected load values were 24.5 kN/m³ self-weight for concrete, 1.3 kN/m² dead load for non-structural elements, 2.2 kN/m² dead load for the unidirectional concrete slab, and 1.5 kN/m² live load (with a 0.5 mass coefficient). Moreover, masonry wall's weight was modelled as distributed loads equal to 6 kN/m or 3 kN/m depending on their thickness. Consequently, the total weight of the building was 33258.6 kN. At the time of the building's construction, horizontal design loads were usually neglected. However, in some particular cases, lateral wind loads equal to 1.5 kN/m² were included. In this case, if the linear base shear due to the wind action is compared to the horizontal first mode seismic action, the effect of both load types is similar, as the ratio between them is close to one. On the contrary, if roof displacements

are compared, the ratio between wind and seismic displacements is 0.59. It means that, in fact, the real problem of this kind of buildings under lateral loads is the lateral displacement control, especially due to seismic actions. For this reason, the analysis of the nonlinear behavior of these buildings is very important, and especially, the evaluation of the rotation capacity of the joints, necessary to reach the displacement demand.

3.3 Nonlinear seismic evaluation

3.3.1 Pushover analysis

In this section, the results of Modal Pushover Analysis (MPA) [40] are presented. Figure 13 includes the capacity and demand curves for the two considered scenarios. First, the behavior of the undamaged structure has been evaluated, Figure 13(a). Afterwards, it has been compared to the worst corrosion conditions obtained in section 3.1, which showed that chloride induced corrosion initiated 15 years after construction, and damage has been accumulated during 40 years of corrosion, Figure 13(b). Both figures include the Response Spectrum (RS) and the Capacity curves according to a Lateral Uniform Load (U), and lateral loads according to the first (M1), second (M2) and third (M3) modes for each situation.

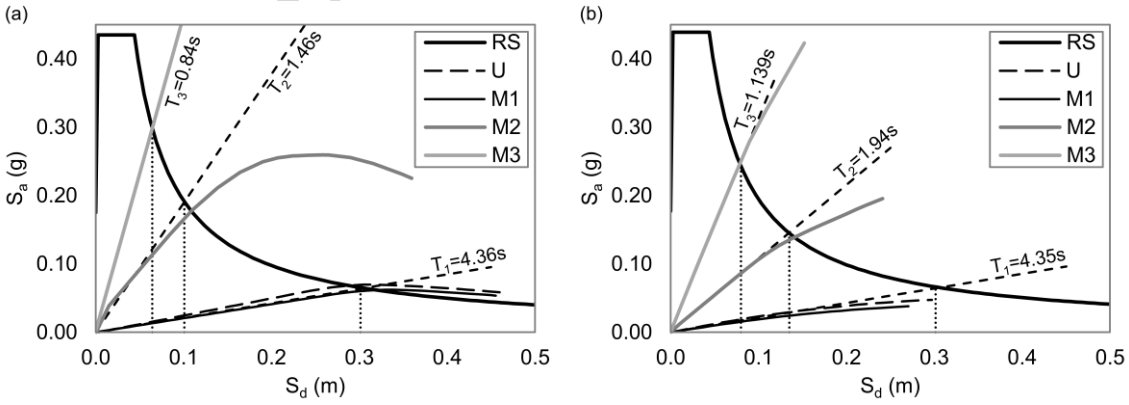

Figure 13. Capacity and demand curves for (a) undamaged and (b) corroded models. ADRS.

Regarding the global seismic evaluation of the building, the performance point was determined according to EC-8, as the intersection between the capacity and demand

curves in the acceleration-displacement response spectrum (ADRS). This method is a simplified version of the N2 method proposed by Reinhorn [46], and doesn't take into account the influence of cumulative damage due to hysteretic cycles, and considers time-independent displacement shape [47], [48]. However, for a proper pushover analysis, in this research, four different load patterns were considered (proportional to the mass distribution of modes 1 to 3 shapes). Moreover, due to the high elastic period of the first mode of vibration, during a real seismic time history analysis, the influence of hysteretic behavior (e.g. concrete-rebar bonding or anchorage loss) should not be important due to the small number of cycles [34]. Therefore, pushover analysis is a suitable method for the analysis of this kind of buildings. Another important point of MPA is the evaluation of the seismic demand according to the equal displacement rule, for medium and long-period range, as the same horizontal displacement demand for the equivalent elastic period (T* for equivalent bilinear model) in the elastic response spectrum. In particular, due to the high value of the elastic period, T, and the small difference with the displacement results for T*, the value of T was used as seismic demand in all models corresponding to the non-corroded structure. However, for the damaged structure, the period corresponding to cracked stiffness, due to the effect of the vertical loads in the initial stiffness, was considered. The curves in Figure 13 show both periods, for the original and cracked sections, and each corrosion scenario. The maximum displacement is equal to the last point of the curve, except for pushover curves with post negative slope. In these cases, according to EC-8, the maximum lateral displacement of the last story corresponds to the point with a 20% strength loss (with respect to the maximum strength).

Figure 13(a) includes the capacity-demand curves for the undamaged structure, in which all four load patterns showed a linear behavior up to the performance point. Moreover,

all capacity curves showed a negative slope after the maximum base shear strength. Figure 14(a) includes the plastic hinge patterns corresponding to MPA of the undamaged structure for each load pattern. First, uniform and mode 1 load patterns showed a small yielding process near the performance point, hinges were located at the beams between the first and fifth stories, and this mechanism increased until the collapse of the structure. However, plastic hinges appeared close to the performance point, and ductility was negligible for the seismic load evaluated in this paper, thus the elastic response spectrum was not reduced due to ductility effect. Finally, none of the structural elements showed any problems due to shear strength, and plastic hinges did not appear in any column or shear wall at the performance point.

On the other hand, the seismic behavior of the damaged structural model (after 40 years of active chloride corrosion) showed a couple of differences. First, the natural frequencies of the second and third modes were reduced, hence the seismic displacement demands were increased, as shown in Figure 13(b). This effect was induced by the new hinges on the beams of Zone 1 (the highest marine exposure), not only in the lower stories but along the whole façade. In addition, Figure 14(b) shows the hinge distribution corresponding to the four load patterns of the corroded model, in which the new hinges at the marine front appeared because of gravity loads and corrosion effect. However, these damages did not affect the natural frequencies for mode 1 or uniform load pattern, despite new hinges in the upper stories appeared in addition to those in the undamaged structure. The second effect of rebar corrosion was the reduction of the displacement capacity for all modes, especially for the first mode and the uniform load shape, in which the performance point was not even reached. In this case, corrosion limited the plastic rotation capacity of the hinges of RC beams, consequently with a bending strength loss on columns and beams, especially in Zone-1

elements (highest Cl^- exposure). Actually, the most important difference between both models was the existence of plastic hinges in zone-1 columns, which were not generated in the original model. Figure 14 summarizes the hinge distribution for each loading pattern of the undamaged and corroded structures (four levels of rotation have been distinguished for plastic damages equal to 25%, 50%, 75% and 100% of the plastic rotation capacity of the hinges). Obviously, the level of structural damage was higher as the mechanical strength of RC sections was affected by corrosion.

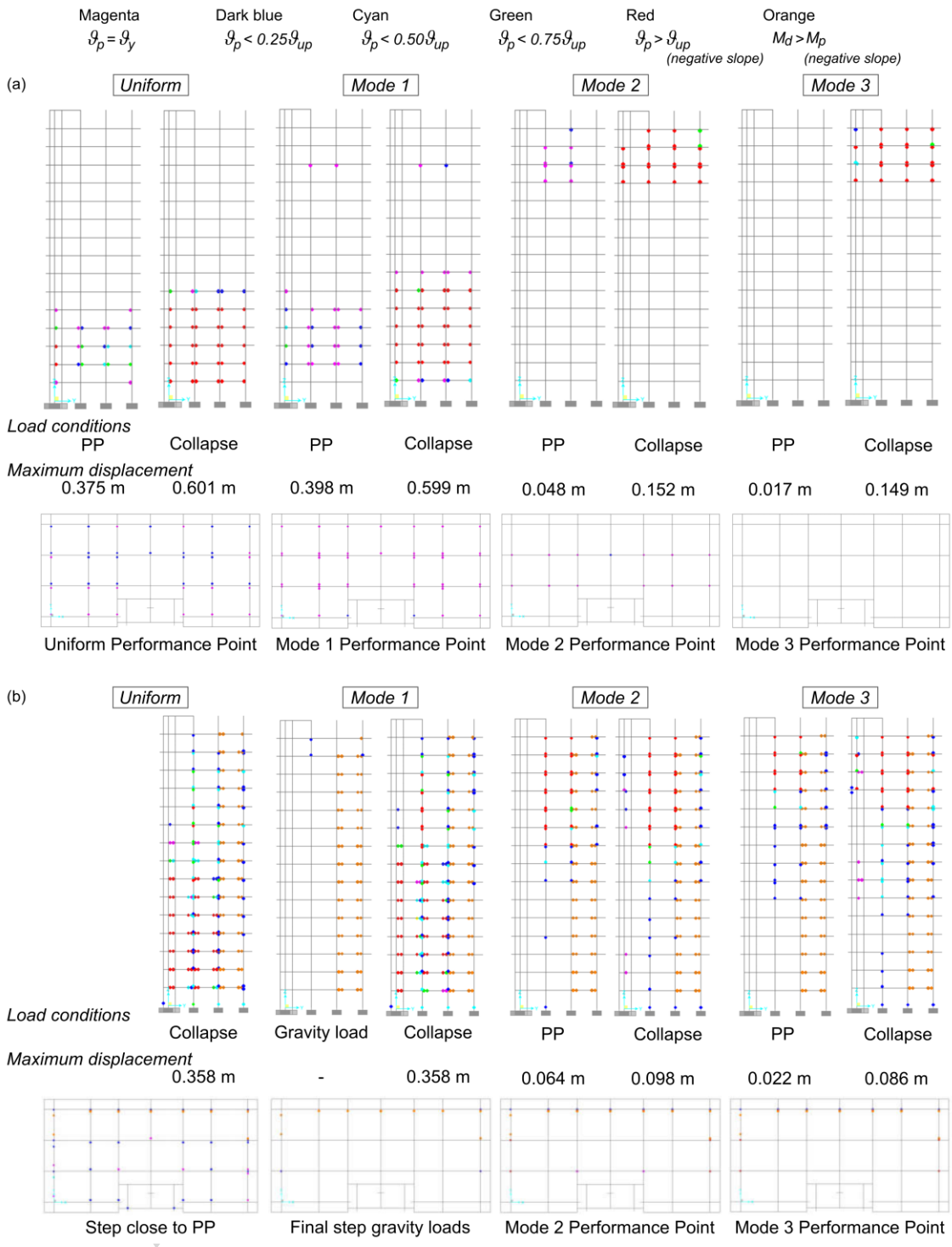

Figure 14. Plastic hinge patterns for modal and uniform load patterns of (a) the undamaged structural model, and (b) with corroded RC sections.

3.3.2 Local ductility and global displacement evaluation.

Finally, the ductility level compatible with the spectrum defined in the MPA must be checked. The methodology proposed in EC-8 has been selected in order to evaluate the

seismic global and local capacity of this kind of building before and after the corrosion attack. First, interstory drifts were limited according to Eq. (11), in which d_r is the maximum value of the interstory drift (i.e. the difference between the average lateral displacements in the mass center of the top and bottom of the story); h is the story height; ν is the reduction factor (equal to 0.5, considering the lower return period of the seismic action associated with the damage limitation requirement); and α_0 depends on the type of non-structural elements and their arrangements into the structure. In particular, this variable α_0 can be assumed equal to 0.005, 0.0075 and 0.010 for buildings with brittle or ductile behavior, or without nonstructural elements in contact with the main structure, respectively.

$$\frac{d_r}{h} \leq \frac{\alpha_0}{\nu} \tag{11}$$

Figure 15 includes the relative drift variation along the height of the building for each load shape. The drift of the corroded structure could not be assessed because the performance point was not reached for all load distributions (first mode and uniform pattern). Hence, the structural safety of the building could not be assured for the assumed corrosion damage. On the other hand, the models (MPA and uniform loading) of the undamaged structure also presented some problems to accomplish the limit values of standards for the stories below the ninth floor, and especially under the fourth. Nonetheless, these limitations refer to nonstructural elements, thus no collapse problems have been detected for this building.

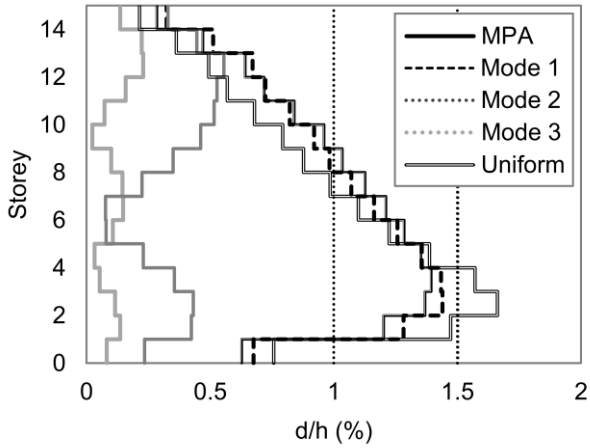

Figure 15. Relative drift distribution for seismic evaluation.

In addition, the local ductility capacity should be controlled [16]. For this purpose, the minimum value for the local ductility demand in relation to the curvature capacity can be determined using Eq. (12). In particular, μ_ϕ has been considered as the ratio between the total curvature capacity and the idealized yield curvature (included in Table 2). β depends on the ductility level and is equal to 3 or 4.5 for medium or high ductility structures. α_u and α_1 are the pushover forces corresponding to the structural collapse and the first hinge step, respectively. The ratio α_u/α_1 needs to be less than 1.5, and in this case, a 1.3 value has been assumed according to EC-8 recommendations for this kind of structures.

$$\mu_{\phi LIM} = 2 \cdot q_0 - 1 = 2 \cdot \beta \cdot \frac{\alpha_u}{\alpha_1} - 1 \tag{12}$$

Eq. (12) is valid for buildings with the first bending frequency in the constant velocity part of the elastic response spectrum, and it is very useful to evaluate the nonlinear capacity of RC sections and to compare the ductility and the rotation capacity of concrete hinges. Figure 16 includes the local ductility μ_ϕ and the evaluation criteria $\mu_\phi/\mu_{\phi LIM}$, for the main concrete sections with and without the effect of corrosion. First, the undamaged sections of the columns up to the sixth floor (CS-1 and CS-2) presented ductility values lower than 25% of the minimum value for medium ductility

level, according to EC-8 [16]. Higher floors showed better ductility due to the reduction of the axial load, but in any case was enough to reach the minimum value for medium ductility class, 6.8. These results were expected according to the design rules during 1960's. Regarding the ductility capacity of non-corroded beams, an approximately constant value equal to 57% for positive bending, BS-1(+) and BS-2(+), was obtained, Figure 15. However, for negative bending, BS-1(-) and BS-2(-),the ductility capacity was significantly reduced, especially for section BS-2, due to the high level of steel rebars, the small depth of concrete section and the insufficient level of lateral confinement (which could have improved the concrete compressive strength). Finally, shear walls showed a 50% approximately value similar to positive bending value for beams.

This limitation value predicts a similar behavior compared to the results of the numerical models. In particular, if the local ductility demand is compared with the global ductility capacity of the building, it can be seen that the relationship between collapse and plastic roof displacement was 1.51 and 1.6 for mode 1 and uniform load patterns, respectively. These values were slightly lower than the global ductility factor recommended in the Spanish standard for low ductility structures, which is equal to 2. Therefore, the non-corroded numerical model showed a similar ductility behavior for mode 1 and uniform load patterns, in comparison with European and Spanish standards.

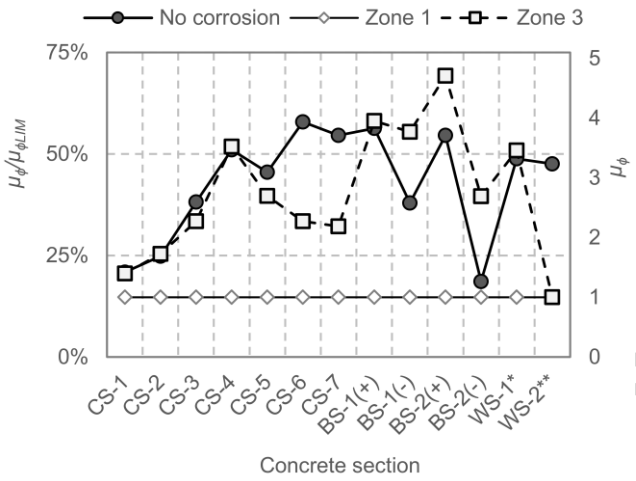

Figure 16. Local ductility evaluation for concrete sections, considering medium ductility class (EC-8).

On the other hand, zoning defined in Figure 10 should be consider to evaluate the corrosion effect in local ductility capacity. Zone 2 has been considered as non-corrosion affected area after the analysis presented in section 3.1. Regarding Zone 1, all elements showed a high level of corrosion and therefore, a high level of reduction coefficient for ductility and strength was applied, and then, brittle behavior was considered (i.e. without ductility), Table 4. In particular, bending strength was reduced between 75% and 90% for beams, and between 65% and 55% for columns, and ductility was equal to 1 for all affected elements, Figure 16. As a summary, localized corrosion due to high chloride attack (zone 1) decreased the bending strength of all exposed structural elements. Besides, plastic hinges were also affected and ductility was reduced. Hence the structural collapse, under seismic accelerations, occurred earlier than in the original model without corroded RC sections.

On the other hand, the RC behavior of zone 3 elements showed a different pattern than their zone 1 counterparts, as the corrosion level is less than 40% for steel rebars with 16 mm diameter or higher. For this reason, the ductility of the steel sections showed values close to 10‰, Figure 9, and the residual bending strength was between 0.5 and 0.74 (with respect to the original strength), Table 4. It is important to remember that the

maximum strain of this kind of steel is 12%, therefore to reduce the maximum EC-8 design strain value (1%) a reduction factor higher than 0.083 would be necessary. This could justify why sections CS-6, CS-7 and WS-2 showed less ductility compared to previous non-corroded sections, Figure 21. Besides, BS-1(-), BS-2(+) and BS-2(-) sections showed higher ductility values, due to the improvement in their plastic rotation capacity. This improvement was due to the high reduction of steel rebar sections and the low reduction of their ductility capacity after corrosion. However, the improvement on plastic rotation capacity of internal beams was not enough to avoid the collapse mechanism of the external columns of the building.

Finally, it is important to highlight that assuming the corrosion hypotheses used in this research, the shear walls conserved enough bending strength to stay on elastic domain during all the seismic action. However, they did not have enough stiffness to reduce the lateral movements when the columns started to yield, and to avoid the collapse mechanism of the corroded structure. Nonetheless, in all the analyses, there were not any problems due to seismic shear stresses.

4. Conclusions.

This study presents a methodology for the structural evaluation of RC buildings in seismic areas near the sea. In this case, a particular problem of coastal residential tall buildings built in 1960's is presented (a singular 15 floors building in Alicante has been selected as an application example of the proposed method). A simplified methodology for the mechanical performance loss because of steel corrosion has been presented, and seismic behavior has been analyzed by modal pushover analyses.

With the aim to analyze the corrosion effect in the structure, several experimental formulations have been implemented, considering national and international concrete codes and recommendations by several authors. First, structural elements are classified

by their exposure level and the residual properties are obtained to update the numerical model. In the studied typology, the differences in chloride or carbonation exposure resulted in an irregular distribution of the mechanical properties along the structure.

The irregular corrosion effect along the building produced an important change in the seismic behavior of the structure. In particular, before corrosion, the analyzed building was safe against the considered seismic loads.

However, after corrosion, the building was not safe against seismic load. In particular, chloride corrosion generated a loss of the global stiffness of the building, and a high reduction of the local ductility of hinges in beams and columns, especially in the elements closer to the marine front. This reduction on the rotation capacity, and the higher demand of horizontal displacement to dissipate the seismic energy, generated an incompatible situation and then, the building collapse due to the failure of the hinges in columns and beams in the most corroded elements.

Moreover, the principal mechanism to dissipate seismic energy was by means of elastic deformation and plastic deformation of beam hinges, and collapse was due to the loss of residual strength during the post negative slope of the beam hinges, with a low grade of ductility, in the same way that explain the standard rules.

It is worth noting that in some elements in the intermediate zone of exposure, the corrosion effect improved the ductility of concrete sections. This was due to the reduction of the mechanical capacity of the steel rebars, and the increase of their plastic deformation. However, this increase in the local ductility was not enough to avoid the seismic collapse of the building, due to the high loss of the rotation capacity in the concrete elements near the marine front.

The described structural typology can be found in several touristic areas in the Mediterranean coast. Therefore, the presented methodology to analyze the effect of

seismic loads on constructions with long exposition to marine environment can be easily applied to other areas.

Acknowledgements

Authors would grateful the City Council of Alicante for the historic information proportionated about the Adoc Tower 7 building.

References

[1] Ministerio de Fomento. Gobierno de España, Norma de construcción sismorresistente: Parte general y edificación (NCSE-02), Real Decreto 997/2002, 27 Septiembre 2002. (2002).

[2] J.G. Ruiz-Pinilla, J.M. Adam, R. Pérez-Cárcel, J. Yuste, J.J. Moragues, Learning from RC building structures damaged by the earthquake in Lorca, Spain, in 2011, Eng. Fail. Anal. 68 (2016) 76–86. doi:10.1016/j.engfailanal.2016.05.013.

[3] Ministerio de la Vivienda. Gobierno de España, Norma M. V. 101-1062, de «Acciones en la edificación»., (1963) Decreto 195/1963, de 17 de enero. BOE núm. 35, pag.

[4] K. Andisheh, A. Scott, A. Palermo, Seismic Behavior of Corroded RC Bridges: Review and Research Gaps, Int. J. Corros. 2016 (2016). doi:10.1155/2016/3075184.

[5] J.D. Moreno, M. Bonilla, J.M. Adam, M. Victoria Borrachero, L. Soriano, Determining corrosion levels in the reinforcement rebars of buildings in coastal areas. A case study in the Mediterranean coastline, Constr. Build. Mater. 100 (2015) 11–21. doi:10.1016/j.conbuildmat.2015.09.059.

[6] K. Tuutti, Corrosion of steel in concrete, Swedish Cem. Concr. Res. Inst. (1982) 469. doi:10.4324/9780203414606_chapter_2.

[7] Y.G. Du, L. a. Clark, a. H.C. Chan, Residual capacity of corroded reinforcing bars, Mag. Concr. Res. 57 (2005) 135–147. doi:10.1680/macr.2005.57.3.135.

[8] A.A. Almusallam, Effect of degree of corrosion on the properties of reinforcing steel bars, Constr. Build. Mater. 15 (2001) 361–368. doi:10.1016/S0950-0618(01)00009-5.

[9] R. Zhang, A. Castel, R. François, Concrete cover cracking with reinforcement corrosion of RC beam during chloride-induced corrosion process, Cem. Concr. Res. 40 (2010) 415–425. doi:10.1016/j.cemconres.2009.09.026.

[10] H. Lin, Y. Zhao, Effects of confinements on the bond strength between concrete and corroded steel bars, Constr. Build. Mater. 118 (2016) 127–138. doi:10.1016/j.conbuildmat.2016.05.040.

[11] H. Yalciner, K. Marar, Experimental Study on the Bond Strength of Different Geometries of Corroded and Uncorroded Reinforcement Bars, J. Mater. Civ. Eng. 29 (2017) 1–10. doi:10.1061/(ASCE)MT.1943-5533.0001914.

[12] A. Meda, S. Mostosi, Z. Rinaldi, P. Riva, Experimental evaluation of the corrosion influence on the cyclic behaviour of RC columns, Eng. Struct. 76 (2014) 112–123. doi:10.1016/j.engstruct.2014.06.043.

[13] Y.C. Ou, L.L. Tsai, H.H. Chen, Cyclic performance of large-sclae corroded reinforced concrete beams, Earthq. Eng. Struct. Dyn. 41 (2012) 593–604.

[14] G.M. Verderame, G. Fabbrocino, G. Manfredi, Seismic response of r.c. columns with smooth reinforcement. Part II: Cyclic tests, Eng. Struct. 30 (2008) 2289–2300. doi:10.1016/j.engstruct.2008.01.024.

[15] P. Sarkar, A.M. Prasad, D. Menon, Seismic evaluation of RC stepped building frames using improved pushover analysis, Earthq. Struct. 10 (2016) 913–938. doi:10.12989/eas.2016.10.4.913.

[16] European Commitee for Standardization, Eurocode 8: Design of structures for earthquake resistance - Part 1 : General rules, seismic actions and rules for buildings, Eur. Comm. Stand. 1 (2004). doi:[Authority: The European Union per Regulation 305/2011, Directive 98/34/EC, Directive 2004/18/EC].

[17] California seismic safety commission, Applied Technology council (ATC40). Seismic evaluation and retrofit of concrete buildings, 1996.

[18] Federal Emergency Management Agency - USA, Prestandard and commentary for the seismic rehabilitation of buildings (FEMA356), (2000) November.

[19] J. Calavera-Ruiz, Proyecto y cálculo de estructura de hormigón, Madrid, 2008.

[20] P. Darwell, F. Allen, Lateral load effective width of flat plates with drop panels, ACI J. 8 (1984) 613–617.

[21] V. Živica, Influence ofw/c ratio on rate of chloride induced corrosion of steel reinforcement and its dependence on ambient temperature, Bull. Mater. Sci. 26 (2003) 471–475. doi:10.1007/BF02707343.

[22] M.B. Otieno, H.D. Beushausen, M.G. Alexander, Modelling corrosion propagation in reinforced concrete structures - A critical review, Cem. Concr. Compos. 33 (2011) 240–245. doi:10.1016/j.cemconcomp.2010.11.002.

[23] A. Scott, M.G. Alexander, The influence of binder type, cracking and cover on corrosion rates of steel in chloride-contaminated concrete, Mag. Concr. Res. 59 (2007) 495–505. doi:10.1680/macr.2007.59.7.495.

[24] J. Warkus, M. Brem, M. Raupach, BEM-models for the propagation period of chloride induced reinforcement corrosion, Mater. Corros. 57 (2006) 636–641. doi:10.1002/maco.200603995.

[25] J. Gulikers, M. Raupach, Numerical models for the propagation period of reinforcement corrosion: Comparison of a case study calculated by different researchers, Mater. Corros. 57 (2006) 618–627. doi:10.1002/maco.200603993.

[26] T. El Maaddawy, K. Soudki, A model for prediction of time from corrosion initiation to corrosion cracking, Cem. Concr. Compos. 29 (2007) 168–175. doi:10.1016/j.cemconcomp.2006.11.004.

[27] Ministerio de Fomento. Gobierno de España, Instrucción de Hormigón Estructural (EHE-08), Real Decreto 1247/2008. Madrid 18 Julio 2008. BOE N^{o} 203. (2008) 35176–35178.

[28] C. Andrade, C. Alonso, Test methods for on-site corrosion rate measurement of steel reinforcement in concrete by means of the polarization resistance method, Mater. Struct. 37 (2004) 623–643. doi:10.1007/BF02483292.

[29] J. Rodriguez, L.M. Ortega, J. Casal, J.M. Diez, Assessing structural conditions of concrete structures with corroded reinforcements, in: 4th Int. Congr. Concr. Serv. Mankind, Proc. an Int. Conf., Dundee, UK, 1996.

[30] C. Andrade, C. Alonso, J. Gulikers, R. Polder, R. Cigna, Vennesland, M. Salta, A. Raharinaivo, B. Elsener, Test methods for on-site corrosion rate measurement of steel reinforcement in concrete by means of the polarization resistance method, Mater. Struct. Constr. 37 (2004) 623–643. doi:10.1617/13952.

[31] C.A. Apostolopoulos, V.G. Papadakis, Consequences of steel corrosion on the ductility properties of reinforcement bar, Constr. Build. Mater. 22 (2008) 2316–2324. doi:10.1016/j.conbuildmat.2007.10.006.

[32] CSI, SAP2000. Analysis Reference Manual, CSI Berkeley (CA, USA) Comput. Struct. INC. (2016) 496.

[33] I.G. y M. de E. IGME, Spanish Geological Survey maps, (2016). http://info.igme.es/cartografiadigital/portada/ (accessed December 6, 2016).

[34] P. Fajfar, A Nonlinear Analysis Method for Performance-Based Seismic Design, Earthq. Spectra.

16 (2000) 573–592. doi:10.1193/1.1586128.

[35] A.K. Chopra, R.K. Goel, A Modal Pushover Analysis Procedure to Estimate Seismic Demands for Buildings : A Modal Pushover Analysis Procedure to Estimate Seismic Demands for Buildings : Theory and Preliminary Evaluation, 2001. doi:10.1002/eqe.144.

[36] A.K. Chopra, Dynamics of Structures, 5th Editio, 2016.

[37] CEN, EN 1992-1 Eurocode 2: Design of concrete structures - Part 1-1: General rules and rules for buildings, (2004). doi:978 0 580 73752 7.

[38] J.B. Mander, M.J.N. Priestley, R. Park, Theoretical stress-strain model for confined concrete, J. Struct. Eng. 114 (1988) 1804–1826. doi:10.1061/(ASCE)0733-9445(1988)114:8(1804).

[39] M. Inel, H.B. Ozmen, Effects of plastic hinge properties in nonlinear analysis of reinforced concrete buildings, Eng. Struct. 28 (2006) 1494–1502. doi:10.1016/j.engstruct.2006.01.017.

[40] R. Park, T. Paulay, Reinforced concrete structures, New York, 1975.

[41] M.J.N. Priestley, F. Seible, G.M. Calvi, Seismic Design and Retrofit of Bridges, John Wiley & Sons, Inc., 2007. doi:10.1002/9780470172858.fmatter.

[42] Caltrans, Seismic Design Criteria, 2013.

[43] A.B. Liel, C.B. Haselton, G.G. Deierlein, Seismic Collapse Safety of Reinforced Concrete Buildings. II: Comparative Assessment of Nonductile and Ductile Moment Frames, J. Struct. Eng. 137 (2011) 492–502. doi:10.1061/(ASCE)ST.1943-541X.0000275.

[44] J.D. Moreno-Romero, Efecto del ambiente marino en edificios de segunda residencia en la costa valenciana. Influencia del crecimiento urbanístico y sistemas constructivos., Technical University of Valencia, 2016.

[45] J.M. Adam, J.D. Moreno, M. Bonilla, T.M. Pellicer, Classification of damage to the structures of buildings in towns in coastal areas, Eng. Fail. Anal. 70 (2016) 212–221. doi:10.1016/j.engfailanal.2016.09.004.

[46] A.M. Reinhorn, Inelastic analysis techniques in seismic evaluations, in: P.F. and H. Krawinkler (Ed.), Seism. Des. Methodol. next Gener. Codes, Balkema, Rotterdarm, 1997: pp. 277–287.

[47] H. Krawinkler, G.D.P.K. Seneviratna, Pros and cons of a pushover analysis of seismic performance evaluation, Eng. Struct. 20 (1998) 452–464. doi:10.1016/S0141-0296(97)00092-8.

[48] A. Gupta, H. Krawinkler, Estimation of seismic drift demands for frame structures, Earthq. Eng. Struct. Dyn. 29 (2000) 1287–1305. doi:10.1002/1096-9845(200009)29:9<1287::AID-

EQE971>3.0.CO;2-B.

Highlights:

- Methodology to evaluate seismic behaviour of old concrete buildings.
- Plastic-Hinge capacity modifications along service life in marine environments.
- Ductility reduction due to corrosion effects.
- Non-linear seismic analysis of damaged concrete buildings.
- Qualitative and quantitative evaluation of a real 39 m tall concrete building.